Nelfinavir, A Lead HIV Protease Inhibitor, Is a Broad-Spectrum, Anticancer Agent that Induces Endoplasmic Reticulum Stress, Autophagy, and Apoptosis *In vitro* and *In vivo*

Joell J. Gills,[1] Jaclyn LoPiccolo,[1] Junji Tsurutani,[1] Robert H. Shoemaker,[5] Carolyn J.M. Best,[2] Mones S. Abu-Asab,[3] Jennifer Borojerdi,[1] Noel A. Warfel,[1] Erin R. Gardner,[6] Matthew Danish,[4] M. Christine Hollander,[1] Shigeru Kawabata,[1] Maria Tsokos,[3] William D. Figg,[1,4] Patricia S. Steeg,[2] and Phillip A. Dennis[1]

Abstract

Purpose: The development of new cancer drugs is slow and costly. HIV protease inhibitors are Food and Drug Administration approved for HIV patients. Because these drugs cause toxicities that can be associated with inhibition of Akt, an emerging target in cancer, we assessed the potential of HIV protease inhibitors as anticancer agents.

Experimental Design: HIV protease inhibitors were screened *in vitro* using assays that measure cellular proliferation, apoptotic and nonapoptotic cell death, endoplasmic reticulum (ER) stress, autophagy, and activation of Akt. Nelfinavir was tested in non–small cell lung carcinoma (NSCLC) xenografts with biomarker assessment.

Results: Three of six HIV protease inhibitors, nelfinavir, ritonavir, and saquinavir, inhibited proliferation of NSCLC cells, as well as every cell line in the NCI60 cell line panel. Nelfinavir was most potent with a mean 50% growth inhibition of 5.2 μmol/L, a concentration achievable in HIV patients. Nelfinavir caused two types of cell death, caspase-dependent apoptosis and caspase-independent death that was characterized by induction of ER stress and autophagy. Autophagy was protective because an inhibitor of autophagy increased nelfinavir-induced death. Akt was variably inhibited by HIV protease inhibitors, but nelfinavir caused the greatest inhibition of endogenous and growth factor–induced Akt activation. Nelfinavir decreased the viability of a panel of drug-resistant breast cancer cell lines and inhibited the growth of NSCLC xenografts that was associated with induction of ER stress, autophagy, and apoptosis.

Conclusions: Nelfinavir is a lead HIV protease inhibitor with pleiotropic effects in cancer cells. Given its wide spectrum of activity, oral availability, and familiarity of administration, nelfinavir is a Food and Drug Administration–approved drug that could be repositioned as a cancer therapeutic.

Authors' Affiliations: [1]Medical Oncology Branch, [2]Molecular Therapeutics Program, [3]Laboratory of Pathology, [4]Clinical Pharmacology Program, Center for Cancer Research, National Cancer Institute, Bethesda, Maryland; [5]Developmental Therapeutics Program, Division of Cancer Treatment and Diagnosis, National Cancer Institute; and [6]Clinical Pharmacology Program, Science Applications International Corporation-Frederick, Inc., National Cancer Institute-Frederick, Frederick, Maryland

Received 1/22/07; revised 5/31/07; accepted 6/14/07.

Grant support: Intramural Research Program of the NIH, National Cancer Institute, Center for Cancer Research, and federal funds from the National Cancer Institute, NIH, under National Cancer Institute Contract NO1-CO-12400. The content of this publication does not necessarily reflect the views or policies of the Department of Health and Human Services, nor does mention of trade names, commercial products, or organizations imply endorsement by the U.S. Government.

The costs of publication of this article were defrayed in part by the payment of page charges. This article must therefore be hereby marked *advertisement* in accordance with 18 U.S.C. Section 1734 solely to indicate this fact.

Note: Supplementary data for this article are available at Clinical Cancer Research Online (http://clincancerres.aacrjournals.org/).

J.J. Gills and J. LoPiccolo contributed equally to this work.

Requests for reprints: Phillip A. Dennis, Medical Oncology Branch, Center for Cancer Research, National Cancer Institute, Building 8, Room 5101, 8901 Wisconsin Avenue, Bethesda, MD 20889. Phone: 301-496-0929; Fax: 301-496-0047; E-mail: pdennis@nih.gov.

©2007 American Association for Cancer Research.

doi:10.1158/1078-0432.CCR-07-0161

Approximately 1.4 million people will be diagnosed with cancer in the United States in 2006 (1). The current cost to develop a new cancer drug is estimated around $1 billion and will likely take in excess of 15 years to go from conception to Food and Drug Administration (FDA) approval (2–4). One way to accelerate development and reduce costs is to identify new indications for already approved drugs, which has been referred to as "repositioning" (5, 6). Repositioning takes advantage of available pharmacokinetic and toxicity data on existing drugs, limits risks and costs to pharmaceutical companies, and could expedite the evaluation and movement of new cancer therapies to the clinic.

Agents that inhibit the HIV retroviral protease were first approved for human use in 1993 and are now widely used to treat HIV/AIDS infection, often in combination with other drugs that form highly active antiretroviral therapy. Although dyslipidemia, insulin resistance, and diabetes are common toxicities of HIV protease inhibitors, the maximum tolerated doses and dose-limiting toxicities of HIV protease inhibitors as single agents have not been defined. Because the toxicities associated with HIV protease inhibitors are similar to those observed with inhibition of the phosphoinositide 3-kinase

Downloaded from http://aacrjournals.org/clincancerres/article-pdf/13/17/5183/2295269/5183.pdf by guest on 09 December 2022

(PI3K)/Akt pathway (7, 8), we hypothesized that HIV protease inhibitors might function as Akt inhibitors.

The PI3K/Akt signaling pathway is a prototypic survival pathway that is commonly activated in many types of cancer and often confers a poor prognosis (9, 10). Development of inhibitors of the PI3K/Akt pathway is a major effort within academia, industry, and government. Unfortunately, the time frame for development of these novel inhibitors will likely not provide benefit for patients who currently have cancer.

To accelerate the availability of pathway inhibitors for clinical testing, we screened six clinically approved HIV protease inhibitors and found that three inhibited growth in a wide variety of cancer cell types at concentrations that have been achieved in patients infected with HIV. The most potent HIV protease inhibitor, nelfinavir, exerted pleiotropic biochemical and cellular effects that included induction of endoplasmic reticulum (ER) stress, autophagy, and apoptosis *in vitro* and *in vivo*. These studies provide a rationale to test nelfinavir as an anticancer agent and suggest that drug repositioning could complement traditional drug development in oncology.

Materials and Methods

Cell culture and reagents

H157 and A549 human non–small cell lung cancer cell lines were obtained from National Cancer Institute/Navy Medical Oncology (Bethesda, MD) and the American Type Culture Collection, respectively, and were maintained in RPMI 1640 containing 5% or 10% fetal bovine serum (FBS), at 37°C in a 5% CO_2 atmosphere. MCF-7, SKBR-3, and BT-474 cells were obtained from the American Type Culture Collection. The MCF-7/LCC2 cell line was from the laboratory of Dr. Robert Clarke (Georgetown University Medical Center, Washington, DC) and JIMT-1 were from DSMZ (German Collection of Microorganisms and Cell Cultures). The SKBR-3/Her10 cells were derived by culturing the parental SKBR-3 cells in 10 μg/mL trastuzumab for at least 20 passages. Reduced response to trastuzumab-induced growth inhibition and p27/KIP1 induction was confirmed by 3-(4,5-dimethylthiazol-2-yl)-2,5-diphenyltetrazolium bromide (MTT) assay and immunoblot, respectively. MCF-7, MCF-7/LCC2, and BT474 were grown in IMEM plus 10% FBS; SKBR-3, SKBR-3/Her10, and JIMT-1 cells were grown in DMEM plus 10% FBS. The following HIV protease inhibitors were obtained through the NIH AIDS Research and Reference Reagent Program, Division of AIDS, National Institute of Allergy and Infectious Diseases, NIH: amprenavir, atazanavir sulfate, indinavir sulfate, nelfinavir, ritonavir, and saquinavir. LY294002 was obtained from LC Laboratories. zVAD-fmk was from BIOMOL International, and 3-methyladenine was from Sigma. Primary antibodies for phosphorylated Akt (S473 and T308), total Akt, phosphorylated extracellular signal-regulated kinase (T202/Y204), total ERK, phosphorylated insulin-like growth factor I receptor (IGF-IR; Y1131), total IGF-IRβ, phosphorylated EGFR (Y1068), total epidermal growth factor receptor (EGFR), cleaved/total caspase-3, caspase-7, caspase-8, caspase-9, cleaved/total poly(ADP)ribose polymerase (PARP), and phosphorylated eIF2α (S51) were from Cell Signaling Technology (Beverly, MA). Antibodies to ATF3 and CHOP were from Santa Cruz Biotechnology. The LC3 antibody and LC3-GFP plasmid were kind gifts of Dr. Tamotsu Yoshimori (National Institute of Genetics, Mishima, Japan). Nelfinavir used in the *in vivo* studies was obtained from Pfizer, Inc.

Cell proliferation assays

The inhibition of cell proliferation/viability in non–small cell lung carcinoma (NSCLC) cells was determined using the WST1 assay (Roche). Briefly, H157 or A549 cells were plated at a density of 1,000 per well in 96-well plates in RPMI 1640 + 5% FBS and allowed to grow for 24 h. HIV protease inhibitors dissolved in DMSO were added, and the cells were allowed to grow for an additional 72 h. WST1 reagent was added to the plates according to manufacturer's protocol, and absorbance was read at 450 nm with an ELISA reader (Bio-Tek Instruments). Cell survival was calculated as a percentage of the value of DMSO-treated controls minus the value of untreated cells on day 0. Experiments were done in triplicate and each drug concentration was evaluated in sextuplet wells for any given experiment. Nelfinavir-dependent growth inhibition in drug-resistant and drug-sensitive breast cancer cell lines was assessed as follows: MCF-7, MCF-7/LCC2 (tamoxifen-resistant version of MCF-7), BT474 (naturally tamoxifen-resistant), SKBR-3, SKBR-3/Her10 (trastuzumab-resistant version of SKBR-3), and JIMT-1 cells (isolated from metastatic disease of a trastuzumab-resistant patient) were seeded at 1,000 per well in 96-well plates in their respective growth medium with FBS reduced to 5%. The cells were allowed to grow for 24 h and then treated with 0, 1, 10, or 50 μmol/L nelfinavir in DMSO. After 48 h, cell numbers were assessed by the MTT assay and calculated as a percentage of the growth of DMSO-treated controls. Experiments were done in triplicate with sextuplet wells for each condition.

NCI60 cell line screen

Methods for evaluation of cell growth inhibition in the NCI60 cell line panel were published previously (11, 12). Briefly, HIV protease inhibitors were solubilized in DMSO, diluted into RPMI 1640 + 5% FBS, then added to 96-well plates containing cell lines that were previously cultured for 24 h. Following a 48 h incubation, the medium was removed and the cells were fixed and stained with sulforhodamine B. Unbound dye was removed with five washes of 1% acetic acid and the plates were allowed to air dry. The dye was resolubilized in Tris buffer and the absorbance at 515 nm was measured. The concentration that produced 50% growth inhibition (GI_{50}) compared with a DMSO control, total growth inhibition, or 0% growth, compared with a DMSO control, and the concentration that produced the death of 50% of the cells present at the start of the experiment (LC_{50}) were determined.

DNA fragmentation assay

Cells were plated in 12-well plates at a density of 1.5×10^5 per well and allowed to grow overnight. The following day, cells were treated with 20 μmol/L HIV protease inhibitors or an equal volume of DMSO for 24 or 72 h. Floating and adherent cells were harvested and fixed in cold 70% methanol. Following fixation, cells were stained with 25 μg/mL propidium iodide and 20 μg/mL RNase A in PBS for 30 min at room temperature. Quantification of sub-2N DNA was determined by flow cytometry using a Becton Dickinson FACSort and by manual gating using CellQuest software (FACSort, BD Biosciences). Apoptosis experiments were done in triplicate and were repeated twice.

Cell death assay

Following incubation, cells were harvested by trypsinization and resuspended in a solution of 1 μg/mL propidium iodide in PBS, then immediately acquired on the FL3 channel of a flow cytometer. The propidium iodide–positive population of cells was considered dead, whereas the propidium iodide–negative population was considered viable.

4′,6-Diamidino-2-phenylindole dihydrochloride staining

Following treatment, cells were pelleted and fixed with methanol/acetic acid (3:1), for 30 min at room temperature. A drop of fixed cell suspension was placed on a glass slide and allowed to dry, then covered with a drop of Vectashield mounting medium plus 4′,6-diamidino-2-phenylindole dihydrochloride (Vector Labs) and a coverslip, followed by visualization with a fluorescence microscope.

Immunoblotting

Cells were plated in six-well plates at a density of 5×10^5 per well. The following day, cells were treated with drug or equal volume of DMSO for the indicated times and lysed in 2× lysis buffer as described previously

Downloaded from http://aacrjournals.org/clincancerres/article-pdf/13/17/5183/2295269/5183.pdf by guest on 09 December 2022

(13). For immunoblotting of tumors, frozen tumors were allowed to thaw on ice, then homogenized in radioimmunoprecipitation assay buffer [150 mmol/L NaCl, 1% Igepal CA-630, 0.5% sodium deoxycholate, 0.1% SDS, 50 mmol/L Tris (pH 8.0)] containing 2.5 mol/L β-glycerol phosphate, 0.2 mol/L sodium orthovanadate, 1.25 mol/L sodium fluoride, and 1× protease inhibitor cocktail (Roche Applied Science) using a hand-held Tissue-Tearor homogenizer (Biospec Products). Cell lysates with equal amounts of protein were separated by SDS-PAGE then transferred to polyvinylidene difluoride membranes. The membranes were blocked for 1 h in blocking buffer (1× TBS, 5% milk, 0.1% Tween 20) and placed in primary antibody diluted in 1× TBS, 5% bovine serum albumin, 0.1% Tween 20, overnight at 4°C. The following day, membranes were washed thrice in wash buffer (0.1% Tween 20, 1× TBS). Primary antibody was detected using horseradish peroxidase–linked secondary antibodies and visualized with the enhanced chemiluminescent detection system (Amersham Biosciences). Immunoblot experiments were done at least thrice.

Electron microscopy

H157 cells were double fixed in PBS-buffered glutaraldehyde (2.5%) and osmium tetroxide (0.5%), dehydrated, and embedded into Spurr's epoxy resin. Ultrathin sections (90 nm) were made and double stained with uranyl acetate and lead citrate, and viewed in a Philips CM10 transmission electron microscope.

Transient transfections

NSCLC cells (1×10^6) were transiently transfected with 2 μg of YFP-ER plasmid, which contains the COOH-terminal Lys-Asp-Glu-Leu ER targeting sequence of calreticulin (Clontech Laboratories), or GFP-LC3 plasmid using nucleofector technology (Amaxa). Following transfection, 1×10^6 cells were plated onto glass coverslips in six-well plates in RPMI + 10% FBS. Seventy-two hours after transfection, the medium was removed and replaced with RPMI + 5% FBS then pretreated or not for 1 h with 3-methyladenine, followed by either DMSO or 20 μmol/L nelfinavir for the indicated times. To harvest, coverslips were incubated in 4% formaldehyde, 1× PBS for 15 min, washed with PBS, then mounted with a drop of Vectashield mounting medium containing 4′,6-diamidino-2-phenylindole dihydrochloride (Vector Labs) followed by visualization using a Zeiss 510 LSM confocal microscope.

Growth factor stimulation

H157 and A549 cells were plated at a density of 5×10^5 per well in six-well plates. The following day, cells were pretreated with 20 μmol/L nelfinavir or an equal volume of DMSO for 30 min. Cells were then stimulated or not with 100 nmol/L IGF-I or 100 ng/mL EGF (R&D Biosystems) for 15 min and lysed for immunoblotting.

In vivo studies

Intraperitoneal administration. For studies with H157 cells, 6-week-old male BALB/c AnNCr-nu/nu mice (Charles River Labs) were injected s.c. with 5×10^6 H157 cells in both shoulders and rear flanks. When tumors were palpable, mice were divided into three groups of 10 mice that were given i.p. injections of either the vehicle alone (4% DMSO, 5% polyethylene glycol, 5% Tween 80 in saline) or 50 or 100 mg/kg nelfinavir dissolved in vehicle, once daily on days 1, 2, 3, 4, 7, 8, 10, 11, and 12. Mice were weighed and tumor measurements were made every other day. For studies with A549 cells, 6-week-old male athymic nude mice were injected s.c. with 1×10^7 A549 cells in 150 μL Matrigel (BD Biosciences) in both rear flanks. When tumors reached 200 mm^2, mice were divided into two groups (nine mice per group) that received either 50 mg/kg nelfinavir or vehicle (4% DMSO, 5% polyethylene glycol, 5% Tween 80 in saline) i.p. daily throughout the study. Mice were weighed and tumors were measured thrice weekly.

Intragastric administration. Eight-week-old female BALB/c AnNCr-nu/nu mice (Charles River Labs) were injected s.c. with 5×10^6 H157 cells in both rear flanks. When tumors were palpable, mice were divided into two groups of seven mice per group. Groups were given either vehicle or 100 mg/kg nelfinavir dissolved in 35% ethanol by gavage, once daily, 5 days per week. In all studies, tumor volume was calculated from the formula $v = (ab^2) / 2$, where a is the long axis and b is the short axis. National Cancer Institute (NCI)-Frederick is accredited by Association for Assessment and Accreditation of Laboratory Animal Care International and follows the USPHS Policy for the Care and Use of Laboratory Animals. Animal care was provided in accordance with the procedures outlined in the *Guide for Care and Use of Laboratory Animals* (National Research Council; 1996; National Academy Press; Washington, DC). *In vivo* experiments were conducted under a protocol approved by the NCI Animal Care and Use Committee.

Assessment of *in vivo* pharmacokinetics

To determine plasma concentrations of nelfinavir, 6-week-old female athymic nude mice were given a single i.p. injection of either 50 or 100 mg/kg nelfinavir in 4% DMSO, 5% polyethylene glycol, and 5% Tween 80 in saline. At each time point, blood was collected from three mice in each dose group, under isoflurane anesthesia, by cardiac puncture. Blood was collected in a Becton Dickinson Microtainer serum separator tube (BD) and centrifuged at 15,000 × g for 1 min. Plasma was stored at -80°C until the time of analysis.

Once samples were defrosted at room temperature and vortex mixed, 100 μL of plasma was transferred to a glass tube. Methyl *tert*-butyl ether (500 μL) was added, along with 5 μL of the internal standard solution (amprenavir) followed by vortex mixing (5 min) and centrifugation (5 min at 2,000 × g). The supernatant was transferred to a clean glass tube and dried under desiccated air at 40°C for 10 min. The sample was then reconstituted in 100 μL of mobile phase. Twenty microliters of this solution were injected onto an Agilent 1100 System, and chromatographic separation was achieved with an Agilent Zorbax SB-C8 column (3.0 × 150 mm, 3.5 μm), running an isocratic mobile phase consisting of 62% of 50 mmol/L sodium phosphate buffer (pH 2.5), 5% methanol (JP Baker), and 33% acetonitrile (JP Baker), for a total run time of 20 min. Retention times were 12 and 15.3 min for nelfinavir and amprenavir, respectively. A diode array detector was used for UV detection, monitoring 210 nm for nelfinavir and 265 nm and amprenavir.

Duplicate sets of calibrator samples, along with quality control samples, were analyzed each day, and the concentration of unknown samples was back-calculated using the calibration curve. The range spanned from 25 to 5,000 ng/mL, with 20-fold dilution allowing for measurement of samples up to 100,000 ng/mL. The accuracy and precision of the quality control samples was well within acceptable limits, ranging from -1.53% to 5.64% and 4.76% to 9.74%, respectively.

Pharmacokinetics were evaluated using a noncompartmental approach, using the mean concentration at each time point, within each dose group. The peak plasma concentration (C_{max}) and the time to peak plasma concentration (T_{max}) are reported as observed values. The area under the plasma concentration versus time curve (AUC_{last}) was calculated using the linear trapezoidal method from time zero (at drug administration) to the time of the last sample with measurable drug concentration for each group (C_{last}). Bailer's method was used to assess the variance, allowing for comparison of nelfinavir exposure between the two dose groups (14). The significance of the difference in AUC was evaluated by Z test. A calculated P value of <0.05 was considered to be significant.

Terminal deoxynucleotidyltransferase-mediated nick-end labeling staining

Formalin-fixed, paraffin-embedded tumor sections on glass slides were deparaffinized and hydrated, followed by staining using a commercial peroxidase-linked apoptosis detection kit (Chemicon) according to the manufacturer's instructions. Samples were counterstained with hematoxylin and visualized using bright-field microscopy. Slides were randomized and counted as terminal deoxyribonucleotide transferase–mediated nick-end labeling (TUNEL)–positive nuclei per 40× field.

Statistics

Experimental values were expressed ±SE. Statistical comparison of mean values was done using the Students t test.

Downloaded from http://aacrjournals.org/clincancerres/article-pdf/13/17/5183/2295269/5183.pdf by guest on 09 December 2022

Results

HIV protease inhibitors inhibit proliferation of a broad spectrum of cancer cell types. To determine if HIV protease inhibitors had potential as cancer therapeutics, we screened six FDA-approved HIV protease inhibitors in cell proliferation assays using two NSCLC cell lines (A549 and H157; Fig. 1A). Atazanavir, nelfinavir, ritonavir, or saquinavir inhibited proliferation of H157 cells. Nelfinavir was most potent (GI_{50} 8 μmol/L). These protease inhibitors were effective in A549 cells, except for atazanavir. Nelfinavir was again the most potent (GI_{50} 9 μmol/L). Because nelfinavir, ritonavir, and saquinavir inhibited growth of two NSCLC cell lines, we assessed the spectrum of activity of these HIV protease inhibitors by screening them in the NCI60 cell line panel that contains 60 cell lines derived from nine different tumor types. Nelfinavir, ritonavir, and saquinavir exhibited dose-dependent inhibition of proliferation in all 60 cancer cell lines. Of the three, nelfinavir was the most potent, with an average GI_{50} of

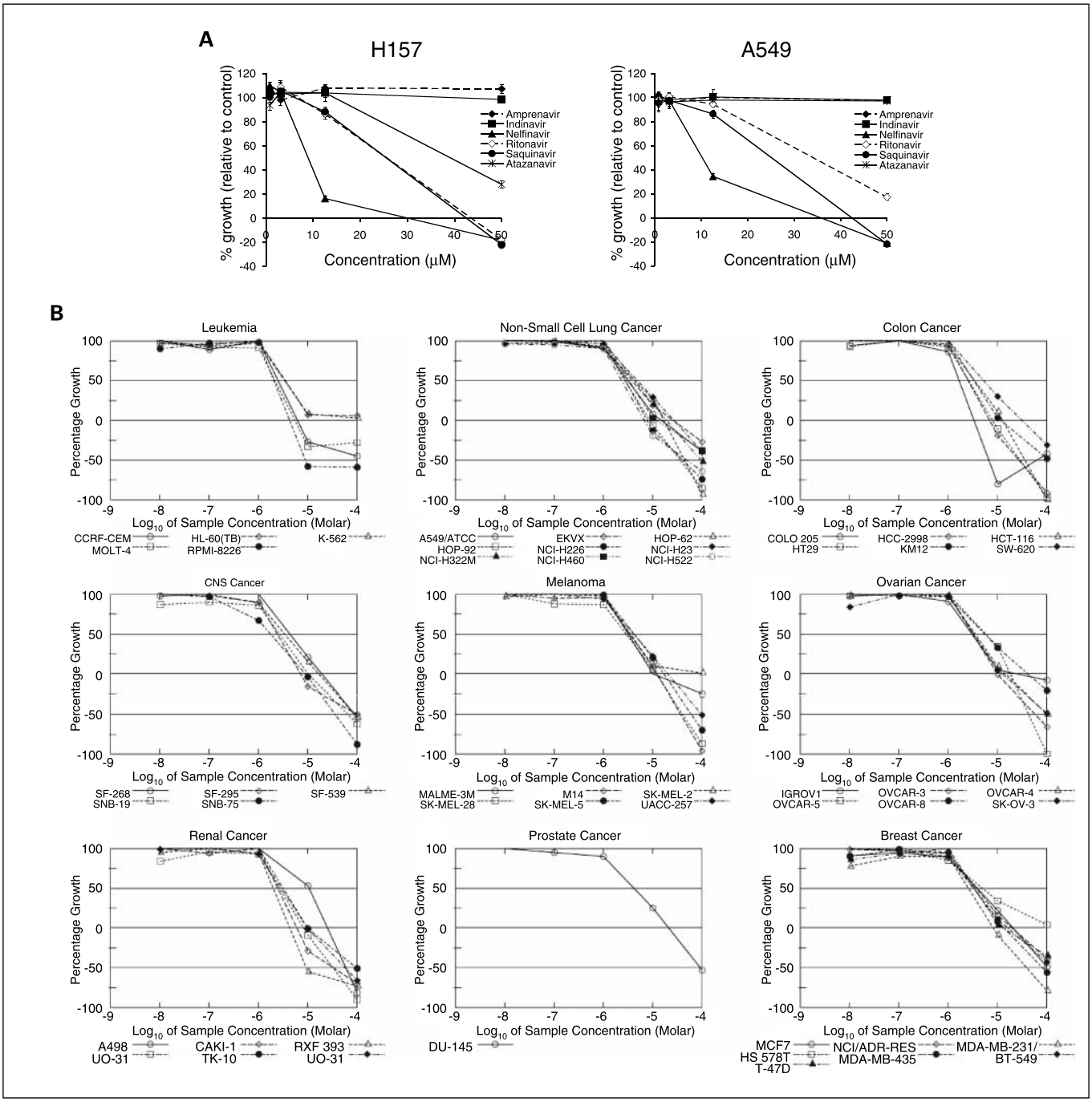

Fig. 1. HIV protease inhibitors inhibit cancer cell proliferation. *A,* WST1 assay for cell proliferation and viability of HIV protease inhibitor – treated H157 (*left*) and A549 (*right*) NSCLC cells. Drug treatments were done in sextuplet and at least three separate assays were done. *B,* growth curves for nelfinavir in the NCI60 cell line panel. Dose-response curves were generated as described in Materials and Methods.

Downloaded from http://aacrjournals.org/clincancerres/article-pdf/13/17/5183/2295269/5183.pdf by guest on 09 December 2022

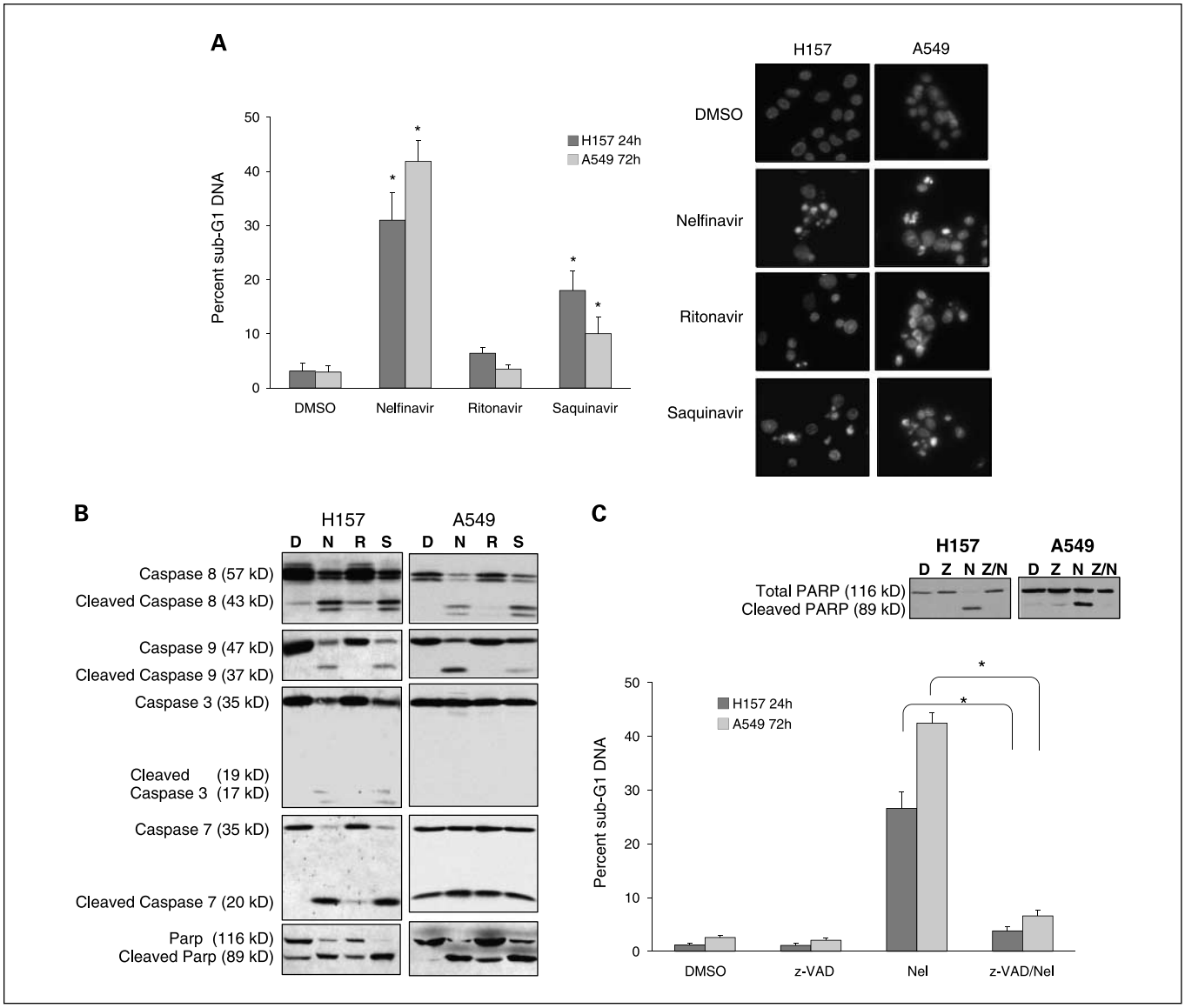

Fig. 2. HIV protease inhibitors induce caspase-dependent apoptosis. *A,* HIV protease inhibitors promote DNA fragmentation and pyknotic nuclei in NSCLC cells. H157 cells and A549 cells were treated for 24 and 72 h, respectively, with DMSO or 20 μmol/L nelfinavir, ritonavir, or saquinavir. Cells were either fixed and stained with propidium iodide, and analyzed for sub-G_1 DNA content by flow cytometry, or fixed and stained with 4′,6-diamidino-2-phenylindole dihydrochloride and visualized by fluorescence microscopy as described in Materials and Methods. *Columns,* mean from two separate experiments; *bars,* SE. *, $P < 0.05$. *B,* HIV protease inhibitors cause caspase cleavage and PARP cleavage. NSCLC cells were treated with DMSO (*D*) or 20 μmol/L nelfinavir (*N*), ritonavir (*R*), or saquinavir (*S*) for 24 h (H157 cells, *left*) or 72 h (A549 cells, *right*). Levels of total and cleaved caspase-3, caspase-7, caspase-8, caspase-9, and PARP were determined by immunoblotting as described in Materials and Methods. *C,* nelfinavir induces caspase-dependent apoptosis in NSCLC cells. NSCLC cells were pretreated or not with the pan-caspase inhibitor zVAD-fmk (50 μmol/L) for 1 h, followed by treatment with DMSO or 20 μmol/L nelfinavir for 24 h (H157 cells) or 72 h (A549 cells). Percentage apoptosis was calculated as the fraction of cells with sub-G_1 DNA content as determined by propidium iodide staining and flow cytometry. *Columns,* mean from at least three separate experiments; *bars,* SE. PARP cleavage was assessed by immunoblotting to confirm inhibition of caspases by zVAD-fmk (*top*). *, $P < 0.01$.

5.2 μmol/L, and cytotoxicity was observed in 14 of 60 cell lines at doses ≤10 μmol/L (Fig. 1B). Despite similar wide spectrums of activity, saquinavir and ritonavir were less potent (Supplementary Figs. S1 and S2, respectively).

HIV protease inhibitors induce caspase-dependent apoptosis. To determine if HIV protease inhibitors were inducing apoptosis, we did a series of biochemical and morphologic assays. In H157 cells, nelfinavir and saquinavir increased the fraction of H157 cells with sub-G_1 DNA content (Fig. 2A). Although nonapoptotic, ritonavir did induce a G_1 cell cycle arrest (data not shown). In A549 cells, HIV protease inhibitor–induced DNA fragmentation was delayed, but the relative potency in A549 cells was the same as in H157 cells (nelfinavir > saquinavir > ritonavir). Because DNA fragmentation has been reported to be associated with both apoptotic and non-apoptotic modes of death, we did 4′,6-diamidino-2-phenylindole dihydrochloride staining to assess HIV protease inhibitor–induced nuclear morphology. Following 24 h treatment in H157 cells or 48 h in A549 cells, pyknotic nuclei were detected after administration of nelfinavir and saquinavir but not ritonavir (Fig. 2A, *right*).

Because caspases activate the endonuclease responsible for cleaving cellular DNA during apoptosis, we did immunoblotting to detect cleavage of caspase-3, caspase-7, caspase-8, and caspase-9

Downloaded from http://aacrjournals.org/clincancerres/article-pdf/13/17/5183/2295269/5183.pdf by guest on 09 December 2022

by HIV protease inhibitors (Fig. 2B). Nelfinavir and saquinavir increased the cleaved forms and decreased the full-length forms of caspase-3, caspase-7, caspase-8, and caspase-9 in H157 cells. Ritonavir had little effect on caspase cleavage, consistent with the lack of DNA fragmentation and induction of G_1 arrest previously noted. Similar results were observed in A549 cells, except that cleavage of caspase-3 and caspase-7 was less apparent. In each cell line, nelfinavir and saquinavir caused the most PARP cleavage.

To assess whether caspase activation was required for nelfinavir-induced death, we used a pan-caspase inhibitor (zVAD-fmk) and measured sub-G_1 DNA formation and PARP cleavage (Fig. 2C). In each cell line, zVAD blocked nelfinavir-induced DNA fragmentation and PARP cleavage by 90%, indicating that nelfinavir-induced apoptosis is caspase dependent. Similar caspase-dependent mechanisms were observed in H157 cells with saquinavir treatment (data not shown).

Nelfinavir induces caspase-independent death, ER stress, and autophagy. In the course of these experiments, we observed that nelfinavir caused profound vacuolization and cellular detachment that occurred even after administration of zVAD-fmk (Fig. 3A). To determine if nelfinavir could induce nonapoptotic cell death, we measured the ability of treated cells to exclude the dye propidium iodide. Nelfinavir induced a 6- to 7-fold increase in uptake of propidium iodide in H157 and A549 cells at 24 and 72 h, respectively (Fig. 3B). When each cell line was pretreated with zVAD, PARP cleavage was inhibited (data not shown), but uptake of propidium iodide was only inhibited by ~10%, indicating that nelfinavir is able to induce nonapoptotic cell death under conditions where caspases are inhibited.

To better define the morphologic changes induced by nelfinavir, transmission electron microscopy was done on H157 cells treated with DMSO (Fig. 3C, a, c, and e) or nelfinavir (b, d, f, g, and h). These studies showed that nelfinavir caused distortion of mitochondria shape with loss of inner membrane integrity (a and b), nucleolar degradation (c and d), decreased glycogen content (*arrowheads*, e and f), and cytoplasmic vacuolization (g). A degradative autophagosome containing cellular organelles was also observed (h).

Because HIV protease inhibitors can increase expression of genes involved in ER stress, and because interruption of the ER secretory pathway can cause ER to distend into visible vacuoles (15, 16), we assessed induction of ER stress in lung cancer cells after administration of nelfinavir. To determine if the vacuoles were ER derived, H157 or A549 cells were transiently transfected with a fluorescent construct containing the ER-targeting sequence of calreticulin and treated with nelfinavir for 12 h (Fig. 3D). In each cell type, nelfinavir caused aggregation of the ER-specific marker into vacuoles that colocalized with the vacuoles evident in phase-contrast microscopy. This suggested that the vacuoles were derived from ER. To confirm activation of ER stress by nelfinavir, we assessed the time-dependent induction of two markers of ER stress, phosphorylation of eIF2α, and expression of ATF3 (Fig. 3E). Increased phosphorylation of eIF2α was evident by 30 min and increased until 6 h, which was observed in both cell types. Expression of ATF3 lagged behind phosphorylation of eIF2α but was also increased in both cell lines by 6 h. Nelfinavir increased phosphorylation of eIF2α and expression of ATF3 to a greater extent than that observed with ritonavir or saquinavir. Together, these data show that induction of ER stress is an early event.

ER stress can trigger autophagy (17, 18), and we observed an isolated autophagosome in our electron microscopy studies. To determine if nelfinavir was inducing autophagy, we did immunoblotting for the microtubule-associated protein 1 light chain 3 (LC3; Fig. 4A). LC3 can exist as a cytoplasmic form (LC3-I) or a membranous form (LC3-II) that only associates with autophagosomes and is a marker for autophagy (19). Nelfinavir increased expression of LC3-I and LC3-II in H157 and A549 cells after 24 h, with greater induction of LC3-II. Pretreatment with zVAD-fmk increased nelfinavir-induced LC3-II expression in H157 cells, but did not change nelfinavir-induced LC3-II expression in A549 cells. zVAD-fmk alone did not affect LC3 expression. These data show that nelfinavir induces a marker of autophagy, LC3-II. To confirm that nelfinavir was inducing autophagy, a GFP-LC3 construct was transfected to label autophagosomes (19). In H157 and A549 cells, nelfinavir increased the number and size of fluorescent LC3 aggregates (Fig. 4B). These fluorescent LC3 aggregates did not colocalize with the vacuoles evident in the phase-contrast micrographs. Additional evidence that these fluorescent aggregates were autophagosomes was derived from experiments showing that pretreatment of cells with 3-methyladenine, an inhibitor of class III PI3Ks and autophagy (20, 21), prevented nelfinavir-induced formation of fluorescent autophagic vesicles. Collectively, these studies show that nelfinavir can induce morphologic and biochemical features of autophagy in NSCLC cells.

To generalize our observations of nelfinavir-induced ER stress followed by autophagy, we assessed time-dependent expression of markers of ER stress (phosphorylated eIF2α, ATF3, and CHOP) and autophagy (LC3, beclin-1) after nelfinavir administration in NSCLC, breast, and prostate cancer cell lines (Fig. 4C). Markers of ER stress increased first. Phosphorylation of eIF2α was increased by 2 h in all but the H460 cells. Expression of ATF3 was increased by 2 h in A549 and PC3 cells. Increased CHOP expression was not evident until 24 h. In contrast to early induction of markers of ER stress, increased LC-3 II expression was only observed at 24 h in all five cell lines, and beclin-1 levels did not change with nelfinavir treatment. The fact that only one marker of autophagy, LC-3 II, changed with nelfinavir treatment is consistent with the observations that different cellular mechanisms are used to induce autophagy after ER stress or starvation (17), and that induction of beclin-1 and LC-3 II can vary depending on the mechanism of induction of autophagy (22). These data suggest that nelfinavir induces a common mechanism of action where ER stress is followed by autophagy.

Effect of HIV protease inhibitors on Akt activation. Because autophagy is a process of energy generation that can be used by cells under conditions of nutrient deprivation or inhibition of the Akt/mammalian target of rapamycin pathway (23), we assessed effects of nelfinavir, ritonavir, and saquinavir on basal levels of Akt activation (Fig. 4D, *left*). Nelfinavir and saquinavir decreased Akt phosphorylation at S473 and T308 within 30 min in H157 cells (*top left*). Total levels of Akt were not affected. Inhibition of Akt activation by either HIV protease inhibitor was less than that observed with a known PI3K inhibitor (LY294002), and was transient, as levels of phosphorylated Akt returned to baseline at 6 h. In A549 cells, inhibition of endogenous Akt activation by HIV protease inhibitors was delayed, first observed at 24 h (*bottom left*). At 48 h, levels of S473 and T308 phosphorylation were further

Downloaded from http://aacrjournals.org/clincancerres/article-pdf/13/17/5183/2295269/5183.pdf by guest on 09 December 2022

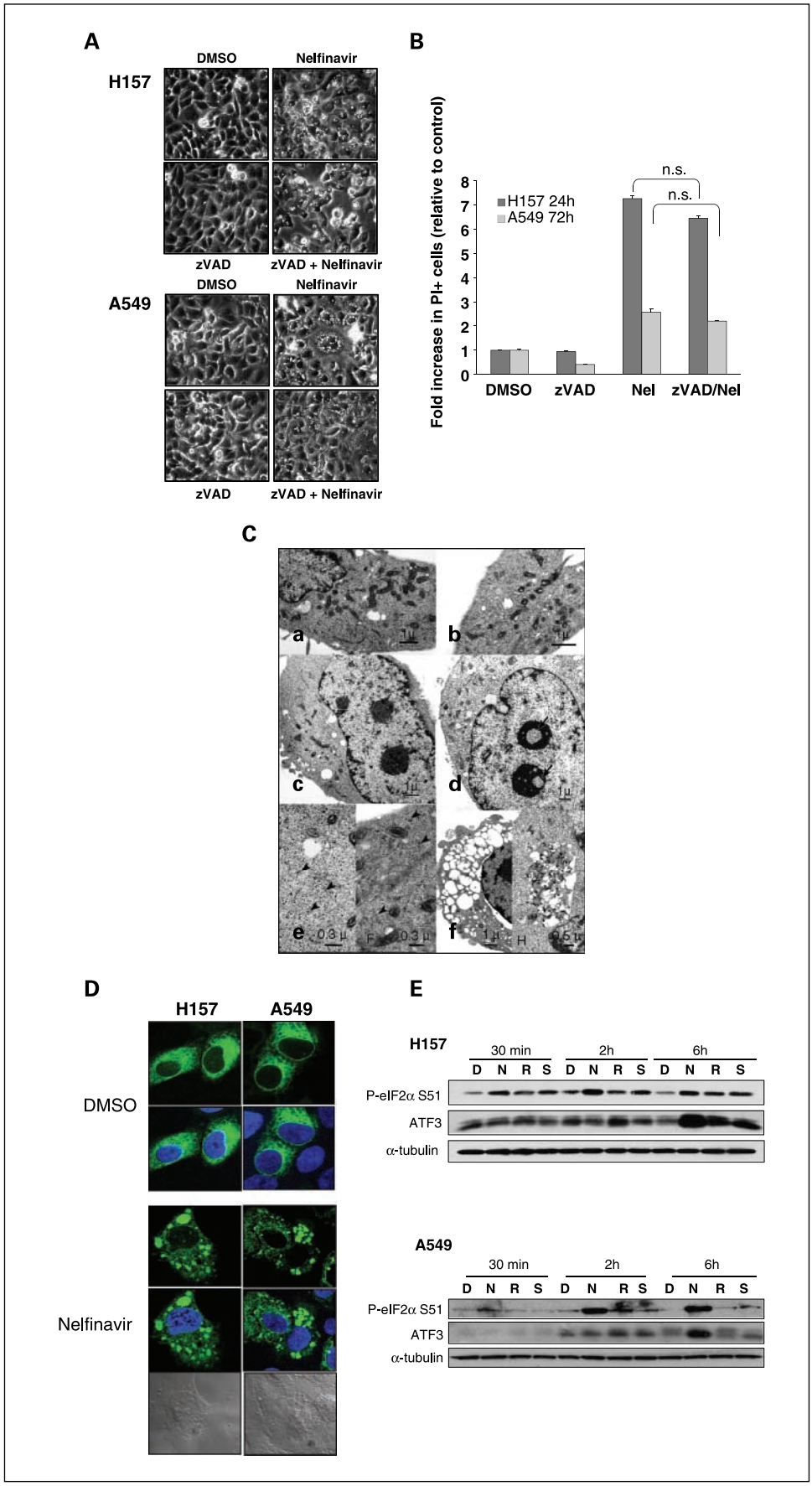

Fig. 3. Nelfinavir induces caspase-independent vacuolization and ER stress. *A,* nelfinavir induces cellular vacuolization in the presence or absence of a pan-caspase inhibitor. NSCLC cells were pretreated with or without zVAD-fmk (50 μmol/L) for 1 h, followed by treatment with DMSO or 20 μmol/L nelfinavir. Phase-contrast micrographs were taken 12 h after nelfinavir treatment. *B,* caspase activation is not required for nelfinavir-induced cell death. NSCLC cells were treated as described in (*A*) for 24 h (H157) or 72 h (A549). Following incubation, cells were assessed for inhibition of dye uptake as described in Materials and Methods. The propidium iodide – positive population of cells was considered dead, whereas the propidium iodide – negative population was viable. *C,* transmission electron microscopy of nelfinavir-treated H157 cells. Cells were treated with DMSO (*a, c,* and *e*) or 10 μmol/L nelfinavir (*b, d, f, g*, and *h*) for 16 h. *a* and *b,* normal versus nelfinavir-treated mitochondria; *c* and *d,* a comparison of nuclear and nucleolar morphology; *e* and *f,* cytoplasmic glycogen content; *g,* a nelfinavir-treated cell with vacuolated cytoplasm; *h,* a degradative autophagosome containing cellular organelles. *D,* nelfinavir induces aggregation of ER that colocalizes with vacuoles. H157 and A549 cells were transfected with a construct containing an ER membrane marker fused to enhanced yellow fluorescent protein, as described in Materials and Methods, and treated with nelfinavir for 12 h. *E,* biochemical markers of ER stress. Immunoblotting for levels of phosphorylated eIF2α and ATF3 was done after variable times of exposure to DMSO, nelfinavir, ritonavir, or saquinavir.

Downloaded from http://aacrjournals.org/clincancerres/article-pdf/13/17/5183/2295269/5183.pdf by guest on 09 December 2022

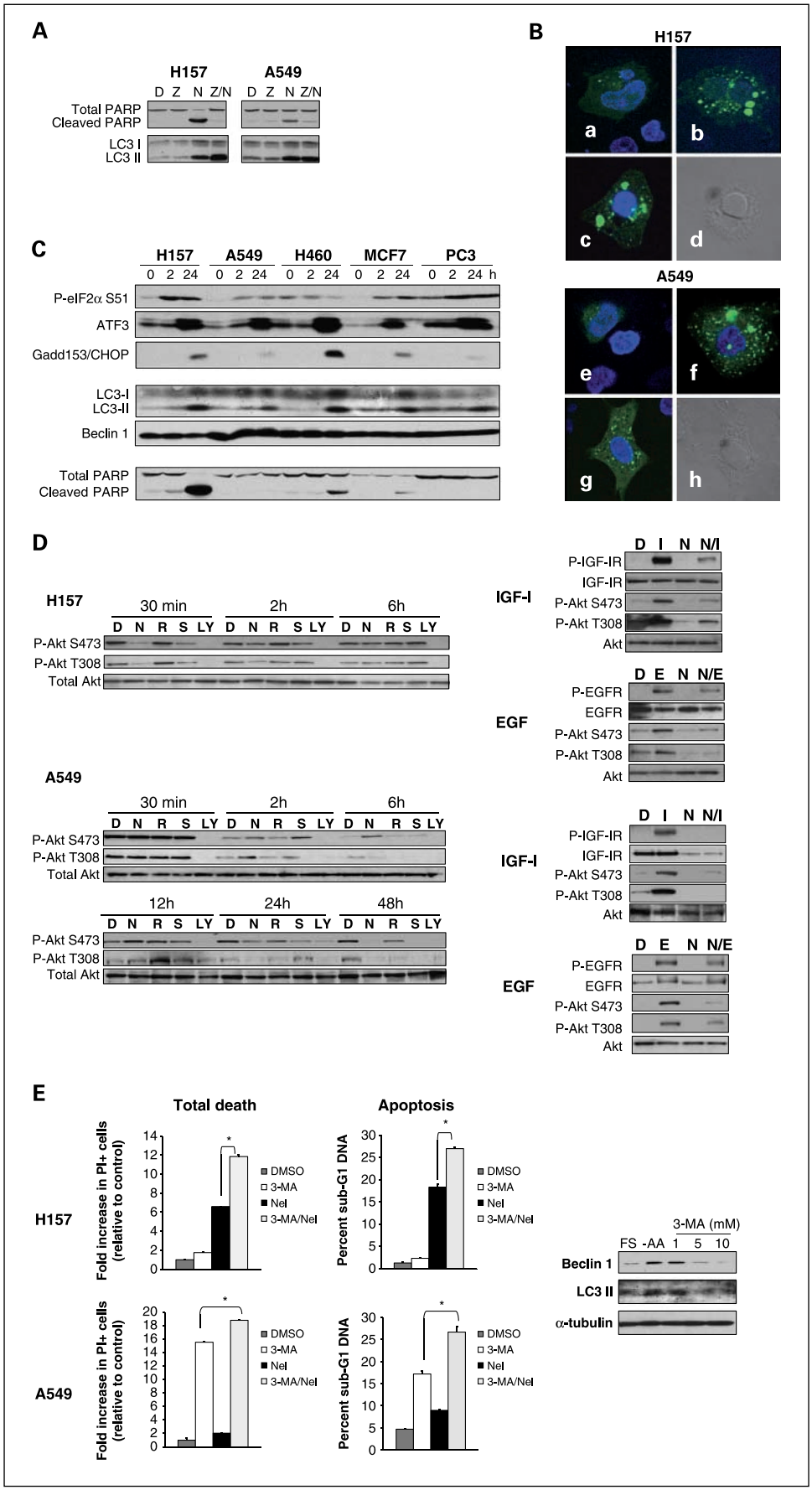

Fig. 4. Effects of nelfinavir on autophagy and Akt activation. *A,* nelfinavir induces expression of LC3-II, a marker of autophagy, independently of caspase activity. Cells were treated and harvested 24 h after nelfinavir treatment. Levels of total/cleaved PARP and LC3 were determined by immunoblotting. *B,* nelfinavir induces LC3 aggregation, which does not overlap with cellular vacuoles. H157 and A549 cells transiently transfected with a GFP-LC3 construct, then treated with DMSO or 20 μmol/L nelfinavir for 24 h. Two separate representative fluorescent images are shown for H157 (*a* and *b*) and A549 (*e* and *f*). Side-by-side fluorescent and phase-contrast images reveal that GFP-LC3 aggregation does not colocalize with vacuoles in H157 (*c* and *d*) or A549 cells (*g* and *h*). *C,* induction of ER stress and autophagy is a common mechanism of action for nelfinavir. Cell lines were treated with DMSO or nelfinavir for the times shown, and immunoblotting was done for markers of ER stress and autophagy. *D,* nelfinavir inhibits basal levels of Akt activation (*left*) and growth factor – induced Akt activation (*right*). H157 or A549 cells were treated with DMSO, or 20 μmol/L nelfinavir, ritonavir, or saquinavir, or 10 μmol/L of the PI3K inhibitor LY294002 (*LY*) for the indicated times. Levels of phosphorylated Akt (S473 and T308) and total Akt were determined by immunoblotting as described in Materials and Methods. For growth factor stimulation, cells were pretreated with DMSO or 20 μmol/L nelfinavir, followed by stimulation or not with IGF-I (*I*; 100 nmol/L) or EGF (*E*; 100 ng/mL) for 15 min. Levels of phosphorylated IGF-I receptor (Y1131), total IGF-Iβ receptor, phosphorylated EGFR (Y1068), total EGFR, phosphorylated Akt (S473 and T308), and total Akt were determined by immunoblotting as described in Materials and Methods. *E,* pretreatment with an inhibitor of autophagy potentiates nelfinavir-induced death. H157 and A549 cells were pretreated or not with 10 mmol/L 3-methyladenine (*3-MA*) for 1 h, followed by treatment with DMSO or 20 μmol/L nelfinavir for 16 h (H157) or 48 h (A549). Total death and apoptosis were measured as described in Materials and methods. *Columns,* mean from at least three separate experiments; *bars,* SE. *, $P < 0.01$.

Downloaded from http://aacrjournals.org/clincancerres/article-pdf/13/17/5183/2295269/5183.pdf by guest on 09 December 2022

reduced after HIV protease inhibitor administration. The greatest reductions in levels of phosphorylated Akt were observed after exposure to nelfinavir and saquinavir. These experiments show that the ability of HIV protease inhibitors to inhibit activation of Akt is time and cell line dependent. However, the HIV protease inhibitors that are most cytotoxic, nelfinavir and saquinavir, were most effective in inhibiting endogenous Akt activation.

We also assessed the effects of nelfinavir on growth factor–induced signaling (Fig. 4C, *right*). H157 or A549 cells were treated with IGF-I or EGF in the absence or presence of nelfinavir, and activation of the cognate receptor tyrosine kinases and Akt was measured using phosphospecific antibodies (Fig. 4B). In H157 cells, nelfinavir decreased the amount of activated IGF-IR and EGFR in response to IGF-I and EGF treatment (*top right*). Nelfinavir also blocked IGF-I– and EGF-stimulated Akt phosphorylation at both S473 and T308. Similar results were observed in A549 cells, where nelfinavir pretreatment inhibited growth factor–induced activation of IGF-IR, EGFR, and Akt (Fig. 4B, *right*). These data show that nelfinavir can inhibit signaling to Akt from two types of receptor tyrosine kinases, IGF-IR and EGFR. Moreover, it suggests that nelfinavir can act at the level of the plasma membrane to inhibit growth factor receptor activation, which subsequently inhibits the PI3K/Akt pathway.

Induction of autophagy counteracts cytotoxicity of nelfinavir. Autophagy can be activated after ER stress to promote survival (17). To assess whether nelfinavir-induced autophagy contributed to cell death, we measured nelfinavir-induced cell death in the absence or presence of 10 mmol/L 3-methyladenine (Fig. 4E). When combined with nelfinavir in H157 cells, 3-methyladenine increased levels of apoptotic and total death. In A549 cells, 3-methyladenine alone was toxic. Nonetheless, the combination of 3-methyladenine and nelfinavir resulted in greater than additive levels of total death and apoptosis. To show that 3-methyladenine was inhibiting autophagy, cells were nutrient deprived of amino acids and the effects of 3-methyladenine on expression of LC3 and beclin-1 were assessed (Fig. 4E, *right*). Amino acid deprivation increased expression of LC3-II and beclin-1, but incubation with increasing concentrations of 3-methyladenine inhibited induction of LC-3-II and beclin-1, indicating that the 3-methyladenine was active and capable of inhibiting autophagy in these cell lines. Collectively, these studies show that autophagy is a cellular response that mitigates nelfinavir-induced death.

Nelfinavir inhibits growth of drug-resistant cancer cell lines. Because nelfinavir was active against all the cell lines in the NCI60 and was broadly active against receptor tyrosine kinase signaling pathways that can promote therapeutic resistance, we tested nelfinavir in a panel of drug-sensitive (MCF-7 and SKBR-3) and drug-resistant breast cancer cell lines (MCF-7/LCC2, SKBR-3/Her10, JIMT-1, and BT474; Supplementary Fig. S3). All cell lines, with the exception of the BT474 cells, were inhibited by at least 60% by nelfinavir at 10 μmol/L. Drug-resistant cells were as sensitive as the parental cell lines. These studies indicate that nelfinavir has activity against cancer cells that acquire resistance to therapies such as tamoxifen and trastuzumab.

***Nelfinavir inhibits growth of NSCLC xenografts and induces apoptosis, ER stress, and autophagy* in vivo.** Because nelfinavir was the lead HIV protease inhibitor based on *in vitro* studies, we evaluated its ability to inhibit the growth of H157 and A549 xenografts when given via i.p. injection (Fig. 5A and B) or gavage (Fig. 5C). With i.p. administration, nelfinavir was well tolerated and significantly decreased H157 tumor growth by 61% at day 11 for the 50 mg/kg group ($P = 6.618 \times 10^{-5}$), and 63% at day 11 for the 100 mg/kg group ($P = 0.0001$). In A549 xenografts, i.p. nelfinavir inhibited tumor growth by 48% at day 19 ($P = 0.046$). In the gavage study, two dosing regimens were compared, 100 mg/kg given daily or 50 mg/kg given twice a day. The daily regimen was well tolerated, but the twice daily gavage regimen was not tolerated, leading to significant loss of body weight in both control and nelfinavir-treated mice. Thus, this regimen was discontinued. Similar to the inhibition of tumor growth observed with i.p. administration, oral administration of 100 mg/kg/d nelfinavir decreased H157 tumor growth in a statistically significant manner ($P = 0.0015$).

The pharmacokinetics of nelfinavir were evaluated in mice following i.p. administration of either 50 or 100 mg/kg (Supplementary Fig. S4). Mean peak plasma concentrations (C_{max}) of 23.21 μg/mL (34.96 μmol/L) and 54.33 μg/mL (81.83 μmol/L) were observed at the first measured time point, 30 min after injection of 50 and 100 mg/kg, respectively. Nelfinavir was rapidly cleared, however, because levels dropped to 0.1 μg/mL (0.15 μmol/L) and 3 μg/mL (4.5 μmol/L) for the 50 and 100 mg/kg dose group, respectively, at 4 h. The overall drug exposure during the sampling time was ~2.5-fold higher in mice receiving 100 mg/kg, compared with those that received 50 mg/kg (3,445.53 versus 1,398.26 min μg/mL; $P = 0.04$).

Tumors from the H157 gavage study were harvested and analyzed for biomarker modulation. Nelfinavir increased the number of apoptotic cells in tumor xenografts, as measured by TUNEL staining (Fig. 5D). Electron microscopy of these tumors (Fig. 5E) revealed increased dilation of the ER, as well as the presence of dense material inside double membrane bound vacuoles (*inset, bottom right*), indicating that nelfinavir induced morphologic features of ER stress and autophagy *in vivo*. To confirm that these processes were occurring in the tumors, we did immunoblotting to assess expression of eIF2α phosphorylation, ATF3, and LC3-II (Fig. 5F). Nefinavir increased expression of all these markers in a statistically significant manner. In contrast to markers of ER stress and autophagy, levels of Akt phosphorylation at S473 did not change with nelfinavir administration. Similar modulation of biomarkers was observed in H157 or A549 tumor lysates from mice given i.p. nelfinavir, where markers of ER stress and autophagy were induced but activation of Akt was not (data not shown). These biomarker studies are consistent with our *in vitro* studies with H157 cells that showed that nelfinavir-induced inhibition of Akt was transient, but that nelfinavir-induced phosphorylation of eIF2α and expression of ATF3 and LC3-II were sustained. Moreover, they show that nelfinavir can achieve effective circulating levels by two routes of administration to inhibit tumor growth *in vivo*, and that nelfinavir can induce apoptosis, ER stress, and autophagy in tumor tissues.

Discussion

The need for expedited development of effective cancer therapies is critical. At current rates, ~8 million Americans will die from cancer during the estimated time it will take for a lead compound to be developed into a FDA-approved drug. An

Downloaded from http://aacrjournals.org/clincancerres/article-pdf/13/17/5183/2295269/5183.pdf by guest on 09 December 2022

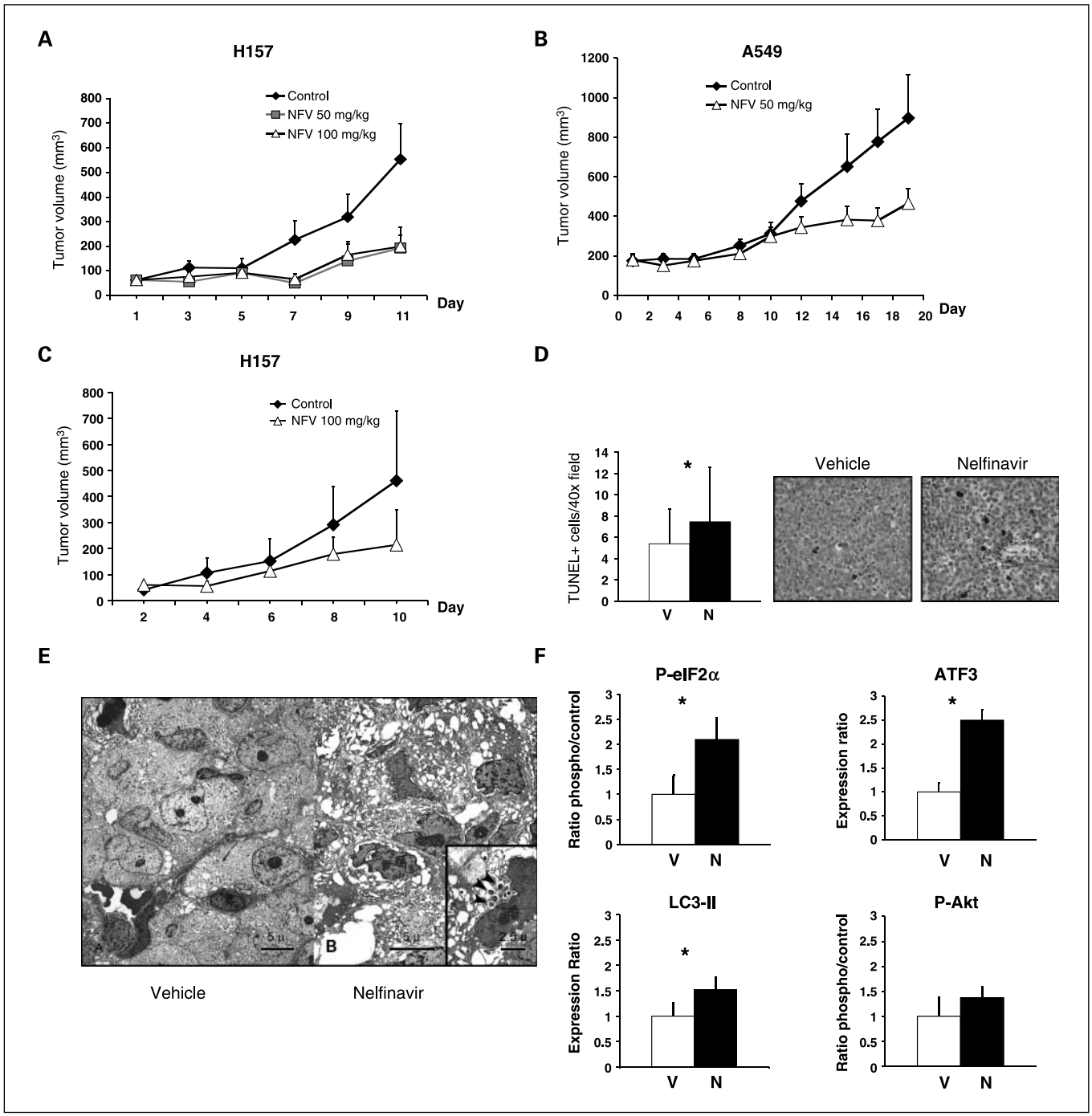

Fig. 5. Nelfinavir inhibits NSCLC tumor growth *in vivo*, and induces markers of apoptosis, ER stress, and autophagy. *A,* H157 cells were grown as xenografts in BALB/c AnNCr-nu/nu mice as described in Materials and Methods. When tumors were palpable, mice were given i.p. injections of vehicle or 50 or 100 mg/kg nelfinavir (*NFV*), once daily, 5 d/wk. *B,* nelfinavir inhibits the growth of A549 xenografts; 1×10^7 A549 cells were injected in 150 μL matrigel in both rear flanks. When tumors reached 200 mm^2, mice were given vehicle or 50 mg/kg i.p. daily throughout the study. *C,* BALB/c AnNCr-nu/nu mice bearing H157 xenografts were given 100 mg/kg nelfinavir or vehicle by gavage, once daily, 5 d/wk. *D,* the number of apoptotic cells per field is greater in tumors from mice given nelfinavir by gavage versus the vehicle control (*$P < 0.05$). Representative photos of TUNEL staining in tumors from mice treated with vehicle or nelfinavir by gavage. *E,* electron micrograph of a vehicle (*left*) and a 100 mg/kg nelfinavir – treated tumor (*right*), harvested from the gavage study. *F,* nelfinavir induces markers of ER stress and autophagy *in vivo*. Tumors were excised from gavage study mice 1 to 2 h following the last dose of nelfinavir and snap frozen. Levels of phosphorylated eIF2α (S51), ATF3, LC3 II, phosphorylated Akt (S473), and α-tubulin were determined by immunoblotting as described in Materials and Methods. Densitometry was done using NIH Image software, and levels of each marker were normalized to α-tubulin for each sample. *, $P < 0.05$.

arguably faster path to development is to reposition established drugs as anticancer agents. Successful examples of this approach include cyclooxygenase-2 inhibitors, which are FDA-approved anti-inflammatory drugs that are approved for cancer chemoprevention in familial adenomatous polyposis patients, and lenalidomide, an analogue of thalidomide, which was originally marketed for morning sickness that is now approved for therapy of myelodysplastic syndromes (24). Other approved

Downloaded from http://aacrjournals.org/clincancerres/article-pdf/13/17/5183/2295269/5183.pdf by guest on 09 December 2022

drugs that are currently under investigation as anticancer agents include the oral hypoglycemic rosiglitazone, the immunosuppressant rapamycin, and the birth control hormone medroxyprogesterone acetate. Collectively, these examples illustrate how repositioning of existing drugs could complement *de novo* drug development.

Could HIV protease inhibitors be repositioned as anticancer agents? Our results in the NCI60 cell line panel show that HIV protease inhibitors have a wide spectrum of activity, inhibiting the proliferation of 60 cancer cell lines derived from nine different tumor types. This is consistent with previous reports demonstrating that HIV protease inhibitors are effective in other model systems such as multiple myeloma and Kaposi sarcoma (25–27). Of the six HIV protease inhibitors evaluated, only three were effective, suggesting that the chemical requirements for HIV protease inhibition and anticancer activity are not identical. Although antitumor effects of many HIV protease inhibitors have been described (28), the two most potent HIV protease inhibitors in our studies were nelfinavir and saquinavir, which produced similar inhibition of proliferation and caused large amounts of apoptosis. Several groups have shown that ritonavir also inhibits the proliferation of cancer cells and our data indicates this is due to a G_1 cell cycle arrest, rather than direct mechanisms of cytotoxicity. Interestingly, both nelfinavir and saquinavir contain a unique *cis*-decahydroisoquinoline-2-carboxamide moiety (Supplementary Fig. S5, *boxed areas*), which could provide a structural basis for the differences in potency between these and other HIV protease inhibitors.

Our data clearly extends the biological mechanisms used by nelfinavir. Although nelfinavir has previously been reported to cause apoptosis and modulate signaling pathways (26, 29, 30), our study shows that nonapoptotic death was also responsible for cytotoxicity in multiple cell lines, including H460, MCF7, and PC3 cells (data not shown). Nonapoptotic cell death was related to induction of ER stress and autophagy in five cancer cell lines, even when apoptosis is blocked. Other cancer agents, such as cisplatin, bortezomib, and 17-(allylamino)-17-demethoxygeldanamycin, also induce ER stress *in vitro* (31–33), but our studies show that nelfinavir induces ER stress *in vivo*. Similarly, several other approved or promising anticancer or chemopreventive agents have been shown to induce autophagy *in vitro*, but none have been shown to induce autophagy *in vivo* (34–36). Thus, our data showing that nelfinavir induces ER stress and autophagy *in vivo* is novel, and implies that markers of ER stress and/or autophagy could be useful in clinical trials with nelfinavir. Whether the induction of autophagy is beneficial for tumor growth or regression is controversial. We used a pharmacologic inhibitor of autophagy, 3-methyladenine, to show that autophagy protected NSCLC cells against nelfinavir-induced death. This suggests that adding an inhibitor of autophagy to nelfinavir might increase its anticancer properties. However, such an approach might also increase toxicity if the induction of autophagy in normal tissues is used as a survival mechanism (37). Of note, we did not observe induction of autophagy in livers from nelfinavir-treated mice (data not shown), suggesting that tumor-specific induction of autophagy could be exploited for therapeutic gain.

Although Akt activation was inhibited by nelfinavir in our studies, the kinetics of inhibition were cell line specific and did not correlate with induction of cellular responses such as ER stress and autophagy. Other groups have reported that nelfinavir decreases phosphorylation of Akt at S473 in cancer cell lines, but only after 1 or 3 days of incubation (26, 29). In addition, other studies have shown that HIV protease inhibitors can inhibit insulin-stimulated Akt activation (26, 38, 39). Our study extends these observations by showing that nelfinavir reduces Akt activation in response to EGF or IGF-I, and that decreased Akt stimulation correlates with decreased receptor tyrosine kinase activation. Mechanistically, this is significant because growth factor receptor activation can be a common means for Akt activation and could be clinically relevant because EGFR and IGF-IR are targets for cancer therapy. Nelfinavir might also have utility in therapeutically resistant tumors because it inhibited proliferation of drug-resistant breast cancer cells in which EGFR and IGF-IR signaling have been implicated in promoting therapeutic resistance (40, 41). These observations are consistent with reports that HIV protease inhibitors can overcome resistance to radiation (29, 42), which can also occur through activation of EGFR and IGF-IR (43, 44).

A recent report by Jiang et al. (45) showed that nelfinavir induces a G_0-G_1 cell cycle arrest in melanoma cells that is related to nelfinavir-mediated degradation of CDC25a, which leads to CDK2 inhibition and dephosphorylation of Rb. In contrast to these results, we did not observe significant alterations in the cell cycle in the five cell lines used in this study (H157, A549, H460, MCF7, PC3; data not shown). Moreover, we did not observe CDC25a degradation, induction of p21 or p27, or decreased levels of cyclin E in H157 or A549 cells. However, in concordance with the results obtained by Jiang et al., nelfinavir decreased phosphorylation of Rb and overall expression of Rb in H157 and A549 cells. This importance of these effects is questionable, however, because decreased phosphorylation and expression of Rb occurred at later time points when most cells were detached and/or dead. Thus, we conclude that alteration of cell cycle distribution is not a primary mechanism of action of nelfinavir in these cell lines.

A key issue in the repositioning of nelfinavir will be the achievable dose in cancer patients. The C_{max} for nelfinavir in HIV patients is ~7 to 9 μmol/L (46, 47), which exceeds the average GI_{50} of 5.2 μmol/L in the NCI60 cell line screen, and suggests that effective concentrations could be achieved in cancer patients. In mice, nelfinavir concentrations peaked at 30 min at 35 or 82 μmol/L for 50 or 100 mg/kg/d dosing, respectively, and levels decreased to 150 nmol/L or 5 μmol/L, respectively, at 4 h. This rapid clearance of nelfinavir is consistent with a half-life of 3 to 5 h in humans when given orally (48), and indicates that tumors were exposed to concentrations that exceed the *in vitro* GI_{50} for <4 h. Given that the dosing regimen for our xenograft studies was daily, it is conceivable that tumors were without drug exposure for prolonged periods everyday, and efficacy could have been improved by more frequent dosing or by the addition of other drugs that retard metabolism of nelfinavir (49). The fact that dose-dependent inhibition of tumor growth was not observed with regimens of 50 or 100 mg/kg/d, despite a 2.5-fold difference in drug exposure over 4 h, suggests that prolonged exposure rather than C_{max} might be more important for tumor inhibition. Notably, establishment of a maximum tolerated dose of nelfinavir as a single agent was never attempted in phase I studies with HIV patients, because dose escalation was stopped once the viral load of HIV decreased.

Downloaded from http://aacrjournals.org/clincancerres/article-pdf/13/17/5183/2295269/5183.pdf by guest on 09 December 2022

Thus, dose escalation above the dose that is FDA approved for HIV patients might be feasible, and a phase I trial using twice daily dosing to establish dose-limiting toxicities and the maximum tolerated dose is now open (NCI-07-C-0047). Achieving higher plasma concentrations than those achieved in HIV patients could maximize the chance for clinical responses, based on dose-dependent effects in the NCI 60 panel, as well as establish the maximum tolerated dose for nelfinavir as a single agent. Given that nelfinavir is a lead HIV protease inhibitor that is orally available and FDA approved with a history of human use, its clinical evaluation as an anticancer agent could be expedited.

Acknowledgments

We thank Gail McMullen for assistance with the animal studies, the NIH AIDS reagent repository, and Pfizer, Inc., for the gift of HIV protease inhibitors; Dr. Tamotsu Yoshimori for the gift of the LC3 antibody and GFP-LC3 plasmid; the Sallie Rosen Kaplan fellowship foundation for support of J.J. Gills and C.J.M. Best; Stephen Wincovitch and Susan Garfield for assistance with confocal microscopy; and Victor Marquez for helpful discussion.

References

1. Jemal A, Siegel R, Ward E, et al. Cancer statistics, 2006. CA Cancer J Clin 2006;56:106–30.
2. Freireich EJ. The Investigational New Drug application—who benefits? Nat Clin Pract Oncol 2006;3:62–3.
3. Mervis J. Productivity counts—but the definition is key. Science 2005;309:726.
4. Drive for drugs leads to baby clinical trials. Nature 2006;440:406–7.
5. O'Connor KA, Roth BL. Finding new tricks for old drugs: an efficient route for public-sector drug discovery. Nat Rev Drug Discov 2005;4:1005–14.
6. Ashburn TT, Thor KB. Drug repositioning: identifying and developing new uses for existing drugs. Nat Rev Drug Discov 2004;3:673–83.
7. Garofalo RS, Orena SJ, Rafidi K, et al. Severe diabetes, age-dependent loss of adipose tissue, and mild growth deficiency in mice lacking Akt2/PKB β. J Clin Invest 2003;112:197–208.
8. Du K, Herzig S, Kulkarni RN, Montminy M. TRB3: a tribbles homolog that inhibits Akt/PKB activation by insulin in liver. Science 2003;300:1574–7.
9. Altomare DA, Testa JR. Perturbations of the AKT signaling pathway in human cancer. Oncogene 2005;24:7455–64.
10. Tsurutani J, Fukuoka J, Tsurutani H, et al. Evaluation of two phosphorylation sites improves the prognostic significance of Akt activation in NSCLC tumors. J Clin Oncol 2006;24:306–14.
11. Monks A, Scudiero D, Skehan P, et al. Feasibility of a high-flux anticancer drug screen using a diverse panel of cultured human tumor cell lines. J Natl Cancer Inst 1991;83:757–66.
12. Monks A, Scudiero DA, Johnson GS, Paull KD, Sausville EA. The NCI anti-cancer drug screen: a smart screen to identify effectors of novel targets. Anticancer Drug Des 1997;12:533–41.
13. Canman CE, Wolff AC, Chen CY, Fornace AJ, Jr., Kastan MB. The p53-dependent G_1 cell cycle checkpoint pathway and ataxia-telangiectasia. Cancer Res 1994;54:5054–8.
14. Bailer AJ. Testing for the equality of area under the curves when using destructive measurement techniques. J Pharmacokinet Biopharm 1988;16:303–9.
15. Parker RA, Flint OP, Mulvey R, et al. Endoplasmic reticulum stress links dyslipidemia to inhibition of proteasome activity and glucose transport by HIV protease inhibitors. Mol Pharmacol 2005;67:1909–19.
16. Mimnaugh EG, Xu W, Vos M, Yuan X, Neckers L. Endoplasmic reticulum vacuolization and valosin-containing protein relocalization result from simultaneous hsp90 inhibition by geldanamycin and proteasome inhibition by velcade. Mol Cancer Res 2006;4:667–81.
17. Ogata M, Hino S, Saito A, et al. Autophagy is activated for cell survival after endoplasmic reticulum stress. Mol Cell Biol 2006;26:9220–31.
18. Yorimitsu T, Nair U, Yang Z, Klionsky DJ. Endoplasmic reticulum stress triggers autophagy. J Biol Chem 2006;281:30299–304.
19. Kabeya Y, Mizushima N, Ueno T, et al. LC3, a mammalian homologue of yeast Apg8p, is localized in autophagosome membranes after processing. EMBO J 2000;19:5720–8.
20. Seglen PO, Gordon PB. 3-Methyladenine: specific inhibitor of autophagic/lysosomal protein degradation in isolated rat hepatocytes. Proc Natl Acad Sci U S A 1982;79:1889–92.
21. Blommaart EF, Luiken JJ, Meijer AJ. Autophagic proteolysis: control and specificity. Histochem J 1997;29:365–85.
22. Matsui Y, Takagi H, Qu X, et al. Distinct roles of autophagy in the heart during ischemia and reperfusion: roles of AMP-activated protein kinase and Beclin 1 in mediating autophagy. Circ Res 2007;100:914–22.
23. Kelekar A. Autophagy. Ann N Y Acad Sci 2006;1066:259–71.
24. Hideshima T, Richardson PG, Anderson KC. Current therapeutic uses of lenalidomide in multiple myeloma. Expert Opin Investig Drugs 2006;15:171–9.
25. Sgadari C, Barillari G, Toschi E, et al. HIV protease inhibitors are potent anti-angiogenic molecules and promote regression of Kaposi sarcoma. Nat Med 2002;8:225–32.
26. Yang Y, Ikezoe T, Takeuchi T, et al. HIV-1 protease inhibitor induces growth arrest and apoptosis of human prostate cancer LNCaP cells *in vitro* and *in vivo* in conjunction with blockade of androgen receptor STAT3 and AKT signaling. Cancer Sci 2005;96:425–33.
27. Ikezoe T, Saito T, Bandobashi K, Yang Y, Koeffler HP, Taguchi H. HIV-1 protease inhibitor induces growth arrest and apoptosis of human multiple myeloma cells via inactivation of signal transducer and activator of transcription 3 and extracellular signal-regulated kinase 1/2. Mol Cancer Ther 2004;3:473–9.
28. Monini P, Sgadari C, Toschi E, Barillari G, Ensoli B. Antitumour effects of antiretroviral therapy. Nat Rev Cancer 2004;4:861–75.
29. Gupta AK, Cerniglia GJ, Mick R, McKenna WG, Muschel RJ. HIV protease inhibitors block Akt signaling and radiosensitize tumor cells both *in vitro* and *in vivo*. Cancer Res 2005;65:8256–65.
30. Pajonk F, Himmelsbach J, Riess K, Sommer A, McBride WH. The human immunodeficiency virus (HIV)-1 protease inhibitor saquinavir inhibits proteasome function and causes apoptosis and radiosensitization in non-HIV-associated human cancer cells. Cancer Res 2002;62:5230–5.
31. Mandic A, Hansson J, Linder S, Shoshan MC. Cisplatin induces endoplasmic reticulum stress and nucleus-independent apoptotic signaling. J Biol Chem 2003;278:9100–6.
32. Nawrocki ST, Carew JS, Pino MS, et al. Bortezomib sensitizes pancreatic cancer cells to endoplasmic reticulum stress-mediated apoptosis. Cancer Res 2005;65:11658–66.
33. Mimnaugh EG, Xu W, Vos M, et al. Simultaneous inhibition of hsp 90 and the proteasome promotes protein ubiquitination, causes endoplasmic reticulum-derived cytosolic vacuolization, and enhances antitumor activity. Mol Cancer Ther 2004;3:551–66.
34. Bursch W, Ellinger A, Kienzl H, et al. Active cell death induced by the anti-estrogens tamoxifen and ICI 164 384 in human mammary carcinoma cells (MCF-7) in culture: the role of autophagy. Carcinogenesis 1996;17:1595–607.
35. Opipari AW, Jr., Tan L, Boitano AE, Sorenson DR, Aurora A, Liu JR. Resveratrol-induced autophagocytosis in ovarian cancer cells. Cancer Res 2004;64:696–703.
36. Raught B, Gingras AC, Sonenberg N. The target of rapamycin (TOR) proteins. Proc Natl Acad Sci U S A 2001;98:7037–44.
37. Lenk SE, Bhat D, Blakeney W, Dunn WA, Jr. Effects of streptozotocin-induced diabetes on rough endoplasmic reticulum and lysosomes of rat liver. Am J Physiol 1992;263:E856–62.
38. Schutt M, Zhou J, Meier M, Klein HH. Long-term effects of HIV-1 protease inhibitors on insulin secretion and insulin signaling in INS-1 β cells. J Endocrinol 2004;183:445–54.
39. Ben-Romano R, Rudich A, Tirosh A, et al. Nelfinavir-induced insulin resistance is associated with impaired plasma membrane recruitment of the PI 3-kinase effectors Akt/PKB and PKC-ζ. Diabetologia 2004;47:1107–17.
40. Nahta R, Yuan LX, Zhang B, Kobayashi R, Esteva FJ. Insulin-like growth factor-I receptor/human epidermal growth factor receptor 2 heterodimerization contributes to trastuzumab resistance of breast cancer cells. Cancer Res 2005;65:11118–28.
41. Knowlden JM, Hutcheson IR, Barrow D, Gee JM, Nicholson RI. Insulin-like growth factor-I receptor signaling in tamoxifen-resistant breast cancer: a supporting role to the epidermal growth factor receptor. Endocrinology 2005;146:4609–18.
42. Maggiorella L, Wen B, Frascogna V, Opolon P, Bourhis J, Deutsch E. Combined radiation sensitizing and anti-angiogenic effects of ionizing radiation and the protease inhibitor ritonavir in a head and neck carcinoma model. Anticancer Res 2005;25:4357–62.
43. Milas L, Raju U, Liao Z, Ajani J. Targeting molecular determinants of tumor chemo-radioresistance. Semin Oncol 2005;32:S78–81.
44. Chinnaiyan P, Allen GW, Harari PM. Radiation and new molecular agents, part II: targeting HDAC, HSP90, IGF-1R, PI3K, Ras. Semin Radiat Oncol 2006;16:59–64.
45. Jiang W, Mikochik PJ, Ra JH, et al. HIV protease inhibitor nelfinavir inhibits growth of human melanoma cells by induction of cell cycle arrest. Cancer Res 2007;67:1221–7.
46. Tebas P, Powderly WG. Nelfinavir mesylate. Expert Opin Pharmacother 2000;1:1429–40.
47. Markowitz M, Conant M, Hurley A, et al. A preliminary evaluation of nelfinavir mesylate, an inhibitor of human immunodeficiency virus (HIV)-1 protease, to treat HIV infection. J Infect Dis 1998;177:1533–40.
48. Pai VB, Nahata MC. Nelfinavir mesylate: a protease inhibitor. Ann Pharmacother 1999;33:325–39.
49. Kurowski M, Kaeser B, Sawyer A, Popescu M, Mrozikiewicz A. Low-dose ritonavir moderately enhances nelfinavir exposure. Clin Pharmacol Ther 2002;72:123–32.

Downloaded from http://aacrjournals.org/clincancerres/article-pdf/13/17/5183/2295269/5183.pdf by guest on 09 December 2022